Research Square

Preprints are preliminary reports that have not undergone peer review.
They should not be considered conclusive, used to inform clinical practice,
or referenced by the media as validated information.

Rumex obtusifolius seed extract and emodin suppress cancer-cell growth via modulation of PI3K/Akt/mTOR and hypoxia-associated signaling

Hayarpi Javrushyan
Yerevan State University
Mery Kocharyan
Yerevan State University
Edita Nadiryan
Yerevan State University
Svetlana Hovhannisyan
Yerevan State University
Gayane Petrosyan
Yerevan State University
Nikolay Avtandilyan
nv.avtandilyan@ysu.am
Yerevan State University
Alina Maloyan
Knight Cardiovascular Institute, Oregon Health & Science University
Mikayel Ginovyan
Yerevan State University

Article

Keywords: Rumex obtusifolius, emodin, PI3K/Akt/mTOR, HIF-1α, MCF-7, A549, MDA-MB-231, cytotoxicity, migration, immunocytochemistry, molecular docking

Posted Date: May 25th, 2026

DOI: https://doi.org/10.21203/rs.3.rs-9762728/v1

License: This work is licensed under a Creative Commons Attribution 4.0 International License.
Read Full License

Additional Declarations: No competing interests reported.

Abstract

Rumex obtusifolius L. seed ethanol extract (ROE) has previously demonstrated anticancer activity in breast and lung cancer models through modulation of cell growth, inflammatory and extracellular-matrix remodeling mediators, and PI3K/Akt-associated survival signaling. The present study aimed to further validate the anticancer activity of ROE and to evaluate emodin, a naturally occurring anthraquinone derivative (a class of aromatic bioactive plant secondary metabolites with quinone-based structure) identified in ROE, as a defined compound-level candidate for mechanistic and translational follow-up. We hypothesized that emodin reproduces key anticancer and pathway-modulating effects of the whole ROE phytochemical matrix, particularly through regulation of PI3K/Akt/mTOR-, hypoxia-, and apoptosis-associated signaling.

Human breast adenocarcinoma MCF-7 cells, triple-negative breast cancer MDA-MB-231 cells, and A549 lung adenocarcinoma cells were cultured under standard conditions (37°C, 5% CO_2) and treated with ROE, emodin, insulin, $CoCl_2$, or pathway-reference compounds depending on the experimental design. Molecular docking, MTT cytotoxicity assay, xCELLigence real-time cell analysis, live-cell membrane-integrity imaging, migration assessment, and immunocytochemistry were used to characterize extract- and compound-level effects.

Docking analysis showed that emodin can be accommodated within functionally relevant binding regions of apoptosis-, inflammation-, and invasion-associated proteins, including Bcl-2, caspase-3, COX-2, and MMP-2, with the strongest predicted affinities observed for COX-2 and MMP-2. In MCF-7 breast cancer cells, ROE reduced viability in a time- and concentration-dependent manner, with an approximate 72-h IC_{50} value of 0.3 mg DW/mL. Real-time impedance monitoring and e-Tox Green imaging further showed that emodin and ROE impaired proliferative fitness and increased the proportion of membrane-compromised cells, consistent with late apoptotic or necrotic cell death, with emodin producing a stronger effect in the real-time assay.

In MDA-MB-231 cells, ROE and emodin moderately attenuated migration-associated cell-index profiles, whereas dactolisib (BEZ235; a dual PI3K/mTOR inhibitor used as a reference in the real-time assay) produced the strongest anti-migratory effect. In A549 cells, emodin reduced insulin-induced pPI3K and pAKT signaling, increased caspase-3 immunofluorescence, and attenuated $CoCl_2$-induced HIF-1α activation. Additional signaling analysis in breast cancer cells supported emodin-associated modulation of mTOR, HIF-1α, and caspase-3 responses.

Together, these findings support ROE as an active anticancer phytochemical matrix and identify emodin as a biologically plausible ROE-associated candidate for further pathway validation, selectivity assessment, formulation optimization, and in vivo anticancer evaluation.

1. Introduction

Natural products remain an important source of anticancer compounds because plant-derived metabolites often affect several interconnected biological processes rather than a single isolated target. This multi-target quality is especially relevant for cancer, where proliferation, apoptosis resistance, inflammatory adaptation, hypoxia tolerance, metabolic remodeling, angiogenesis, and migration are functionally integrated components of tumor progression and therapy resistance [1, 2]. The challenge is to convert complex extract-level activity into a mechanistically interpretable and translationally useful framework. For medicinal plants, this requires parallel confirmation of whole-extract efficacy and identification of constituent compounds that can serve as mechanistic anchors or development candidates.

The PI3K/Akt/mTOR signaling cascade occupies a central position in this framework. It integrates growth-factor input, cellular energy status, survival signaling and biosynthetic control, and it is frequently dysregulated in breast, lung, and other solid tumors. Activation of PI3K and Akt promotes cell-cycle progression, glucose metabolism, anti-apoptotic signaling, epithelial-to-mesenchymal transition, and therapeutic resistance. Downstream mTOR signaling supports protein synthesis and anabolic growth, while crosstalk with inflammatory and hypoxia-associated pathways helps tumor cells adapt to adverse microenvironmental conditions [3]. Therefore, the PI3K/Akt/mTOR axis is not only a therapeutic target but also a mechanistic readout that can connect cytotoxicity, survival signaling and metastatic phenotypes.

Hypoxia is another key determinant of aggressive tumor behavior. Stabilization of HIF-1α enables tumor cells to adapt to low-oxygen conditions by altering metabolism, angiogenic signaling, and survival programs. HIF-1α also contributes to drug resistance and metastatic potential in breast cancer and other solid tumors by interacting with PI3K/Akt/mTOR, VEGF-dependent angiogenic signaling, inflammatory mediators, and matrix-remodeling enzymes [4, 5]. Similarly, COX-2 and MMP-2 represent important functional outputs of inflammation-associated tumor progression. A biologically meaningful anticancer extract would be expected to influence several of these nodes in a coordinated manner.

Rumex obtusifolius L. (broad-leaved dock, Polygonaceae) has been investigated by our group as an Armenian medicinal plant with antioxidant, anti-inflammatory, antimicrobial, and anticancer potential. Earlier work showed that *R. obtusifolius* seed extracts possess antioxidant and biochemical activity [6, 7]. More directly, ROE displayed anticancer activity in cellular and animal models. In a DMBA-induced rat breast cancer model, ROE-based combinations (with nor-NOHA and L-NAME) influenced tumor-related oxidative stress, inflammation, and polyamine metabolism [8].

These findings support ROE as an active anticancer phytochemical mixture, but they also raise a necessary question for development: which compound or class of compounds is responsible for the extract's beneficial effects? In our previous study, ROE was shown to regulate several interconnected cancer-associated endpoints in A549 cells, including TNF-α, VEGF-α, COX-2, MMP-2, total and phosphorylated PI3K/Akt, ROS/RNS-associated parameters, and caspase-3-mediated apoptosis, particularly in combination with 5-fluorouracil [9]. This suggests that the anticancer activity of ROE may

result from coordinated modulation of inflammatory, oxidative-stress, extracellular-matrix remodeling, and cell-survival pathways. That work also introduced an *in silico* prioritization step in which HPLC/MS/MS-identified ROE phytochemicals were docked against the binding pockets of Akt and PI3K, two central nodes of the survival pathway implicated in the observed extract-level response. The docking analysis showed that several ROE constituents had favorable predicted interactions with these targets, with 14 of 17 investigated compounds showing better predicted affinity toward Akt than the redocked Akt control ligand. Among the phytochemicals, four compounds - endocrocin, emodin, luteolin, and quercetin - were prioritized for further binding-mode analysis because they combined strong docking performance with acceptable predicted drug-likeness parameters according to Lipinski-based SwissADME evaluation [9].

Among the prioritized ROE-associated phytochemicals, emodin was selected as a defined candidate compound because it combined favorable predicted interaction with PI3K/Akt-related targets, acceptable drug-likeness, known occurrence in *Polygonaceae*-associated medicinal plants, and published evidence of anticancer activity. Previous studies have linked emodin to inhibition of cancer-cell proliferation, induction of apoptosis, suppression of migration/invasion, and regulation of PI3K/Akt/mTOR, HIF-1α, MAPK, and Bcl-2/caspase-associated signaling [10–16]. Therefore, emodin was used in the present study as a chemically defined ROE-associated compound to evaluate whether it reproduces key anticancer and pathway-modulating features of the extract.

The present study was therefore designed with two linked aims. First, we sought to further confirm the anticancer efficacy of ROE using cell viability, real-time phenotyping, migration, and inflammatory/remodeling readouts. Second, we evaluated emodin as a candidate RO-associated compound for future *in vivo* development by testing whether it reproduces key anticancer phenotypes and modulates PI3K/HIF-1α/caspase-associated signaling. This approach avoids reducing ROE activity to a single molecule, while allowing emodin to be positioned as a tractable mechanistic and translational lead within the broader phytochemical activity of *R. obtusifolius*.

2. Materials and methods

2.1. Chemicals and reagents

Analytical-grade chemicals and cell-culture reagents were purchased from Sigma-Aldrich (USA), Abcam (UK), or certified equivalent suppliers. Emodin was used as the RO-associated reference compound. Dactolisib was used as a PI3K/mTOR-directed positive control in cytotoxicity and migration assays, and doxorubicin was used as a pro-apoptotic comparator in the indicated immunocytochemistry experiments. Primary antibodies used for immunocytochemistry included anti-HIF-1α (Abcam, ab179483), anti-phospho-PI3K (Abcam, ab191606), anti-phospho-AKT (Abcam, ab179463), anti-mTOR (EPR390(N)), Abcam, ab134903, anti-caspase-3 (EPR18297), Abcam, ab184787. Fluorescent secondary antibodies included goat anti-rabbit IgG H&L Alexa Fluor 488 (Abcam, ab150077) and goat anti-rabbit

IgG H&L Alexa Fluor 647 (Abcam, ab150115). DAPI or Hoechst was used for nuclear counterstaining according to the manufacturer's protocol.

2.2. Plant material and extract preparation

Seeds of *R. obtusifolius* L. were harvested from the Tavush region of Armenia at approximately 1400–1600 m above sea level, as described earlier [17]. Plant identification was performed at the Department of Botany and Mycology, Yerevan State University (YSU), and voucher material was deposited at the YSU Herbarium under voucher specimen number ERCB 13208. Permission for sampling was obtained from the landowner. Ground seeds were extracted by maceration with 96% ethanol at a 10:1 solvent-to-sample ratio (v/w), following previously established protocols [8, 9]. The final ethanol concentration in all experimental conditions did not exceed 1% (v/v), and the corresponding vehicle control was included. The crude-extract yield was 10.60 ± 2.31%.

2.3. Phytochemical basis for emodin selection

The selection of emodin was based on the previously characterized phytochemical profile and the earlier *in silico* prioritization of RO-associated metabolites. Published LC-HRMS/HPLC-MS/MS data showed that ROE is a chemically rich extract containing phenolic and anthraquinone-associated constituents [8]. Detailed HPLC/HPLC-MS chromatographic methods, representative chromatograms, peak assignments, and additional phytochemical data related to ROE are provided in the Supplementary Materials. In our previous PI3K/Akt-focused analysis, emodin was among the compounds predicted to interact favorably with pathway-related targets [9]. Emodin was therefore selected as a defined RO-associated molecule for comparison with the whole seed extract.

2.4. Cell cultures

MCF-7 human breast adenocarcinoma cells (ATCC HTB-22), A549 human lung adenocarcinoma cells (ATCC CCL-185), and MDA-MB-231 human triple-negative breast cancer cells (ATCC HTB-26) were obtained from ATCC. MCF-7 and MDA-MB-231 cells were maintained in Eagle's minimum essential medium or the laboratory-validated equivalent, whereas A549 cells were maintained in Dulbecco's modified Eagle's medium [18]. Culture media were supplemented with 10% fetal bovine serum, 2 mmol/L L-glutamine, 200 mg/L sodium pyruvate, 100 U/mL penicillin, 100 µg/mL streptomycin, and, where applicable, 0.25 µg/mL amphotericin B. Cells were grown at 37°C in a humidified atmosphere containing 5% CO2 in the PHCbi MCO-230AICUVL-PA CO_2 incubator. Mycoplasma contamination was monitored using a universal mycoplasma detection kit, and experiments were performed with cell passages 5–15.

2.5. Molecular docking

Molecular docking was performed to evaluate the predicted binding mode of emodin with apoptosis-, inflammation-, and invasion-associated molecular targets. The three-dimensional structures of Bcl-2, COX-2, MMP-2, and caspase-3 were retrieved from the Protein Data Bank (https://www.rcsb.org/). Bcl-2 was selected because its hydrophobic BH3-binding groove mediates interaction with pro-apoptotic BH3-domain proteins and represents a functionally relevant site for small-molecule anti-apoptotic Bcl-2

inhibition. The crystal structure of the Bcl-2 complexed with a small-molecule inhibitor occupying this groove was used for docking analysis (PDB ID: 4MAN), and the co-crystallized ligand was removed before docking.

COX-2 was selected as an inflammation-associated cancer-related target because its overexpression is linked to tumor-cell proliferation, angiogenesis, invasion, metastasis, and apoptosis resistance [19, 20]. The COX-2 crystal structure was obtained from the Protein Data Bank (PDB ID: 1CX2), and the binding pocket was defined within the cyclooxygenase channel before docking. MMP-2 was included as a matrix-remodeling and invasion-associated target. The MMP-2 structure was obtained from the Protein Data Bank (PDB ID: 8H78), and catalytically or structurally relevant metal ions, including Zn^{2+} and Ca^{2+}, were retained during receptor preparation. Caspase-3 was selected as a key apoptosis-associated protease, with particular attention to the active-site region containing functionally important residues such as Cys163 and His121.

Protein structures were prepared using PyMOL by removing water molecules and non-essential heteroatoms, while retaining biologically relevant cofactors or ions when required for structural or catalytic integrity. AutoDock Vina was used to calculate ligand conformations and estimate binding affinities [21]. The resulting docking complexes were visualized using PyMOL to assess the ligand position within the binding pocket. BIOVIA Discovery Studio was used to generate two-dimensional interaction diagrams and to identify conventional hydrogen bonds, carbon–hydrogen bonds, hydrophobic contacts, π–sigma interactions, alkyl/π–alkyl interactions and amino-acid residues contributing to complex stabilization.

2.6. MTT cytotoxicity assay

MTT cytotoxicity assay [22] was performed to evaluate the effect of ROE on MCF-7 breast cancer cell growth and, where indicated, the effects of ROE and emodin on MDA-MB-231 cells. The cells were seeded in 96-well plates and allowed to attach under standard culture conditions before treatment. Cells were then exposed to increasing concentrations of ROE in the range of 0–0.5 mg DW/mL or emodin for 4, 24, or 72 h. Vehicle-treated cells served as controls, and the final vehicle concentration was maintained at a non-toxic level under the applied experimental conditions. After the indicated exposure periods, MTT reagent was added to each well, and cells were incubated to allow formazan formation. Formazan crystals were then solubilized, and absorbance was measured at 570 nm using a SPECTROstar Nano microplate reader (BMG LABTECH, Germany). Cell growth/viability was expressed as a percentage of the corresponding vehicle-treated control (1% ethanol). Three independent experiments were performed with technical replicates. Dose–response curves were generated where applicable, and approximate IC_{50} values were calculated from 72-h curves using nonlinear regression with variable slope.

2.7. Real-time impedance monitoring and live-cell membrane-integrity imaging

MCF-7 cells were seeded in E-Plate 96 wells at 10,000 cells/well and monitored using an Agilent xCELLigence RTCA eSight system (Agilent Technologies, USA) [23]. After recording a cell-free background, cells were seeded in complete medium and allowed to attach for 24 h before treatment. Impedance-derived cell index was recorded every 15 min for up to 96 h and normalized to the start of treatment. Then ROE (0.5 mg DW/mL), emodin (40 μM), and dactolisib (BEZ235, 0.2 μM; positive cytotoxic control) were applied. For live-cell membrane-integrity analysis, e-Tox Green was added together with treatments. Fluorescence was acquired in parallel with impedance measurements, and green fluorescence indicated membrane-compromised late apoptotic or necrotic cells.

2.8. xCELLigence migration assay

Migration of MDA-MB-231 triple-negative breast cancer cells was assessed using the xCELLigence RTCA DP system and CIM-Plate 16 [23]. The lower chamber contained complete medium supplemented with 10% FBS as a chemoattractant. The upper chamber was seeded with 5 × 10^4 MDA-MB-231 cells in low-serum medium containing ROE (0.5 mg DW/mL), emodin (40 μM), and dactolisib (0.2 μM). Dactolisib was used as a PI3K/mTOR-directed reference inhibitor of motility-associated behavior. Real-time migration was monitored for 24 h, and impedance values were converted to Cell Index. Migration-associated Cell Index curves and 24-h area-under-the-curve values were used to compare treatment effects among groups.

2.9. Immunocytochemistry of PI3K/Akt/mTOR and hypoxia-associated signaling

A549 cells were seeded in black 96-well imaging plates at 1.5 × 10^4 cells/well and cultured for 24 h. To activate PI3K/Akt signaling, cells were treated with insulin (200 nM) [23]. Hypoxia-like stress was induced with CoCl2 (200 nM). Emodin was applied (40 μM) as a defined RO-associated compound. After treatment, cells were washed with PBS, fixed with 4% paraformaldehyde, permeabilized with Triton X-100, blocked with bovine serum albumin, and incubated overnight at 4°C with antibodies against pPI3K, pAKT, mTOR, caspase-3, or HIF-1α. Alexa Fluor-conjugated secondary antibodies were then applied, and nuclei were counterstained with Hoechst or DAPI. Images were acquired using a Cytation C10 confocal imaging system (Agilent BioTek, USA). Fluorescence intensity was quantified using Gen5 software and normalized to the corresponding vehicle-treated control. Additional immunocytochemistry experiments were performed in MDA-MB-231 cells to assess HIF-1α, mTOR, and caspase-3 responses under CoCl2-, insulin-, doxorubicin-, and emodin-associated conditions.

2.10. Statistical analysis

All experiments were repeated at least three times independently. Data are presented as mean ± SD or mean ± SEM, as indicated in the figure legends. Group comparisons were performed using one-way or two-way ANOVA, followed by appropriate post hoc multiple-comparison tests. Dunnett's test was used for comparisons with a single control group, whereas Tukey's test was used for multiple pairwise comparisons. Non-parametric alternatives were applied when assumptions of normality were not met.

Statistical analyses were performed using GraphPad Prism 8 software (GraphPad Software, San Diego, CA, USA). A p-value < 0.05 was considered statistically significant.

3. Results

3.1. Emodin shows predicted interactions with apoptosis-, inflammation-, and invasion-associated proteins

Molecular docking indicated that emodin can be accommodated within functionally relevant binding regions of Bcl-2, COX-2, MMP-2, and caspase-3 (Figure 1 and Table 1). Among the analyzed targets, the strongest predicted binding affinity was observed for COX-2, followed by MMP-2, whereas Bcl-2 and caspase-3 showed more moderate predicted binding. This ranking suggests that emodin may preferentially interact with inflammation- and matrix-remodeling-associated targets, while also showing structural compatibility with apoptosis-related proteins.

The predicted COX-2 complex was mainly stabilized by hydrophobic and π-associated contacts within the cyclooxygenase channel, consistent with the favorable accommodation of emodin in an inflammation-associated cancer target. In MMP-2, emodin was positioned within the active-site region and showed a combination of polar and hydrophobic interactions, supporting its potential relevance to invasion- and matrix-remodeling-associated mechanisms. These findings are consistent with the inclusion of COX-2 and MMP-2 as targets linked to tumor inflammation, migration, and metastatic behavior.

For apoptosis-associated proteins, emodin showed moderate predicted interaction with the Bcl-2 hydrophobic BH3-binding groove and with the caspase-3 binding region. The Bcl-2 result supports a possible connection with anti-apoptotic signaling, whereas the caspase-3 docking result should be interpreted cautiously as structural compatibility with an apoptosis-associated protein, not as direct evidence of caspase-3 activation. Functional apoptosis-related conclusions are therefore based primarily on the cellular immunocytochemistry data rather than docking alone. The docking results support the biological plausibility that emodin may interact with apoptosis-, inflammation-, and invasion-associated molecular targets. These in silico findings complement the experimental data by positioning emodin as a mechanistically relevant ROE-associated compound. However, direct target-engagement assays, enzyme-inhibition studies, or other orthogonal validation experiments will be required to confirm functional inhibition of COX-2, MMP-2, or Bcl-2.

3.2. ROE and emodin reduce MCF-7 viability and real-time proliferative fitness

MTT analysis demonstrated that ROE decreased MCF-7 cell growth in a time- and concentration-dependent manner (Figure 2A). The 4-h exposure produced only modest growth inhibition, whereas 24-h

and particularly 72-h treatment caused a pronounced reduction in viability at higher concentrations. Nonlinear regression of the 72-h dose–response curve yielded an approximate IC_{50} value of 0.3 mg DW/mL for ROE, confirming its direct cytotoxic activity in MCF-7 breast-cancer cells. These findings extend our previous ROE studies, in which ROE showed anticancer activity in additional tumor models, including HT29 colon cancer and A549 lung adenocarcinoma cells. In A549 cells, ROE alone did not significantly suppress cell growth at the tested concentrations, but it enhanced the effect of 5-fluorouracil at 4 and 24 h, reduced TNF-α, VEGF-α, COX-2, and MMP-2, downregulated PI3K/Akt signaling, and increased apoptosis-associated readouts, including caspase-3 activity and nuclear condensation/fragmentation [9].. Thus, the current MCF-7 data confirm direct cytotoxic activity of ROE in breast cancer cells, while the earlier A549 data support a broader anticancer profile involving chemosensitization, anti-inflammatory/anti-remodeling effects, PI3K/Akt pathway modulation, and apoptosis induction.

Real-time impedance monitoring confirmed the endpoint MTT data (Figure 2B). Untreated control cells showed a progressive increase in cell index, reflecting continued attachment, spreading, and proliferation. Dactolisib rapidly decreased the cell index after compound addition, validating the assay as a sensitive readout of PI3K/mTOR-associated cytostatic/cytotoxic disruption. Emodin produced a marked suppression of the cell-index profile and strongly reduced the proliferative AUC, indicating pronounced impairment of attachment, spreading, and growth dynamics. ROE showed a more moderate but evident inhibitory effect on proliferative capacity. Live-cell imaging with e-Tox Green further supported these findings, showing increased membrane-compromised cells after emodin treatment, whereas ROE induced a weaker cytotoxic signal. Dactolisib produced the strongest loss of membrane integrity, as expected for the reference PI3K/mTOR inhibitor (Figure 2C). Together, MTT, RTCA, and live-cell imaging confirm that ROE is active against MCF-7 breast cancer cells and that emodin, as a defined ROE-associated anthraquinone, reproduces a key cytotoxic and anti-proliferative component of this phenotype

3.3. ROE and emodin differentially affect MDA-MB-231 viability, proliferative fitness, and migration

In MDA-MB-231 triple-negative breast cancer cells, ROE and emodin showed different activity profiles (Figure 3). MTT analysis revealed that ROE did not markedly reduce cell growth within the tested concentration range, indicating limited direct anti-viability activity under these conditions. In contrast, emodin produced a clear time- and concentration-dependent decrease in cell growth, with the strongest inhibition observed after 72 h. At higher concentrations, emodin reduced cell growth below the IC_{50} threshold, demonstrating stronger anti-viability activity than ROE (Figure 3A).

Real-time impedance monitoring showed a progressive increase in cell index in untreated cells, reflecting continued attachment and proliferation. Dactolisib markedly suppressed the cell-index profile and significantly reduced the AUC, whereas ROE and emodin produced more moderate changes in

proliferation-associated impedance (Figure 3B). Live-cell imaging further supported these findings, showing the strongest e-Tox Green signal after dactolisib treatment, while ROE and emodin also increased the number of membrane-compromised cells compared with untreated controls (Figure 3C).

The migration phenotype was assessed using the xCELLigence CIM-plate system (Figure 3D). Untreated cells displayed a progressive migration-associated increase in cell index over the recording period. Dactolisib caused the clearest reduction in the migration curve and AUC, consistent with the role of PI3K/mTOR signaling in motility-associated behavior. ROE and emodin generated lower migration-associated cell-index trajectories than untreated cells; however, their AUC reductions were modest and did not reach statistical significance. Overall, these data indicate that emodin has stronger direct anti-viability activity in MDA-MB-231 cells, whereas ROE shows weaker but detectable effects on cell behavior. The anti-migratory effects of ROE and emodin remained moderate compared with dactolisib, but were directionally consistent with reduced aggressive cell behavior.

Importantly, the absence of pronounced cytotoxic effects in HREC normal cells at the tested concentrations suggests that the observed biological activity may preferentially affect cancer-associated signaling pathways rather than inducing nonspecific toxicity [24].

3.4. Emodin suppresses insulin-induced PI3K/Akt activation and modulates HIF-1α and caspase-3 in A549 cells

Immunocytochemistry was used to evaluate whether emodin affects growth-factor- and hypoxia-associated signaling in A549 lung adenocarcinoma cells (Figure 4). Insulin stimulation increased pPI3K signal relative to DMSO control, confirming activation of the PI3K pathway. Co-treatment with emodin reduced the insulin-induced pPI3K signal, supporting an inhibitory effect at the level of proximal PI3K activation. Insulin also increased pAKT, while emodin significantly attenuated this response. The mTOR signal increased after insulin stimulation and showed a lower mean value after insulin plus emodin, although the difference between insulin and insulin plus emodin was less pronounced than for pPI3K and pAKT.

Emodin also increased caspase-3 immunofluorescence relative to DMSO control, indicating activation of apoptosis-associated signaling. $CoCl_2$ increased HIF-1α immunofluorescence, confirming induction of a hypoxia-like response, while emodin reduced the $CoCl_2$-associated HIF-1α signal toward control levels. These data indicate that emodin affects two biologically important axes in A549 cells: growth-factor-associated PI3K/Akt signaling and hypoxia-associated HIF-1α stabilization. The simultaneous increase in caspase-3 supports the interpretation that emodin shifts the cellular balance away from survival signaling and toward apoptosis-associated responses.

3.5. Emodin modulates HIF-1α, mTOR and caspase-3 in an additional breast-cancer signaling panel

An additional immunocytochemistry panel was used to assess emodin effects on HIF-1α, mTOR, and caspase-3 in MDA-MB-231 triple-negative breast cancer cells (Figure 5). CoCl2 increased HIF-1α signal relative to control, confirming activation of a hypoxia-like response. The CoCl2 plus emodin condition showed a lower mean HIF-1α signal than CoCl2 alone, indicating partial attenuation of hypoxia-associated signaling in this experimental setting. Insulin increased mTOR immunofluorescence, while insulin plus emodin reduced mTOR signal compared with insulin alone, supporting downstream modulation of the PI3K/Akt/mTOR pathway. In the apoptosis-associated readout, emodin increased caspase-3 signal, exceeding the DMSO control and the doxorubicin comparator in the presented quantification. These findings extend the A549 signaling observations and support emodin as an apoptosis-associated, survival-pathway-modulating candidate compound in breast cancer models.

4. Discussion

The present study provides an extract-to-compound anticancer framework for *R. obtusifolius* seed ethanol extract. The central concept is that ROE represents a reproducibly active anticancer phytochemical matrix, while emodin emerges as a chemically defined candidate compound that reproduces several key anticancer features and can be advanced for deeper mechanistic and *in vivo* evaluation. This work builds directly on our previous ROE studies, where the extract was shown to influence cancer-cell viability, inflammatory and angiogenic mediators, oxidative/metabolic parameters, and PI3K/Akt-associated signaling [8, 9]. The novelty of the present research is therefore not only the confirmation of ROE bioactivity, but the transition from a complex extract-level phenotype toward a rationally selected compound-level candidate. The present findings are consistent with the broader literature describing emodin as a pleiotropic anticancer anthraquinone rather than a single-target cytotoxic compound. Recent reviews summarize that emodin can inhibit cancer-cell proliferation, induce apoptosis, interfere with migration/invasion, and regulate multiple oncogenic pathways, including PI3K/Akt/mTOR, HIF-1α, MAPK, NF-κB, HER2, Bcl-2/Bax and caspase-associated signaling [10, 25, 26]. Therefore, the multitarget profile observed in the present study is biologically plausible and fits well with the established pharmacological behavior of emodin. The value of our data is that these mechanisms are linked here to a defined *R. obtusifolius* seed-extract context and compared directly with the whole ROE phytochemical matrix.

In the present study, ROE reduced MCF-7 cell viability, impaired real-time proliferative fitness, and increased membrane-compromised cells, confirming direct anticancer activity in a breast cancer cell model. These findings are consistent with our earlier work, where ROE showed broader anticancer behavior through modulation of tumor-associated inflammation, angiogenesis, matrix-remodeling mediators, and PI3K/Akt signaling. In particular, ROE-associated regulation of COX-2 and MMP-2 has

already been demonstrated in previous studies and is therefore used here primarily as a mechanistic background rather than as the main new endpoint of the present study [23].

Emodin provides a mechanistic and translational entry point into this phytochemical matrix. The RTCA data (which captures dynamic changes in cell adhesion, spreading, and proliferation that cannot be fully resolved by endpoint viability assays) demonstrate that emodin has substantial antiproliferative/cytotoxic activity. The increase in e-Tox Green-positive cells further indicates treatment-associated membrane compromise, compatible with late apoptosis or necrosis. Together with increased caspase-3 immunofluorescence, these data support an apoptosis-associated component of emodin activity. This interpretation is consistent with the broader emodin literature, where emodin has been associated with modulation of Bcl-2/Bax balance, caspase activation, and apoptosis induction in several tumor models [10, 14]. The apoptosis-associated component of emodin activity is also supported by earlier lung cancer studies. In A549 lung adenocarcinoma cells, Su et al. showed that emodin induced apoptosis through a reactive oxygen species-dependent mitochondrial pathway, accompanied by cytochrome c release, caspase-2, caspase-3, and caspase-9 activation, AKT/ERK inactivation, decreased mitochondrial Bcl-2, and increased mitochondrial Bax [27]. This is directly relevant to our A549 data, where emodin increased caspase-3 immunofluorescence and reduced insulin-induced PI3K/Akt signaling. Thus, our results are consistent with a model in which emodin suppresses survival signaling while promoting apoptosis-associated responses.

The docking analysis provides a structural rationale for the experimentally observed anticancer activity of emodin. Emodin showed the most favorable predicted binding to COX-2 and MMP-2, two proteins associated with inflammation-driven tumor progression, matrix remodeling, and invasive behavior. Its predicted interaction with the Bcl-2 BH3-binding groove further supports a possible connection with apoptosis regulation, whereas the moderate interaction with caspase-3 is consistent with the apoptosis-associated experimental phenotype but should not be interpreted as direct proof of caspase-3 activation. Importantly, the docking data should be considered supportive and hypothesis-generating. They strengthen the mechanistic plausibility of emodin as a RO-associated anticancer candidate, but direct biochemical target-engagement assays, enzyme-inhibition studies, or orthogonal validation experiments will be required to confirm functional inhibition of COX-2, MMP-2, or Bcl-2. The KEGG and protein–protein interaction analyses further support this pathway-level interpretation. Recent work by Yuan et al. used Cytoscape-based PPI analysis, GO/KEGG enrichment, molecular docking, molecular dynamics, and experimental validation to investigate emodin in prostate cancer, identifying the caspase pathway as a core target [15]. Although performed in a different cancer model, that study supports the use of KEGG/PPI analysis to interpret emodin as a network-level anticancer modulator.

The most important signaling observation is that emodin modulated insulin- and hypoxia-associated PI3K/Akt/mTOR signaling in A549 cells. Reduction of pPI3K by emodin is mechanistically meaningful because it places the compound upstream in a survival pathway already implicated in ROE activity. In parallel, emodin increased caspase-3 signal and reduced $CoCl_2$-induced HIF-1α, suggesting that it acts at the intersection of growth-factor signaling, hypoxia adaptation, and apoptosis-associated response. In

cancer cells, PI3K/Akt activation supports survival, metabolic adaptation, and resistance to stress, while HIF-1α contributes to hypoxia-driven angiogenic and pro-metastatic phenotypes. By modulating pPI3K/HIF-1α signaling and increasing caspase-3-associated apoptosis, emodin shifts the cellular response toward a less adaptive and more apoptosis-prone state. Recent A549-based evidence further supports the relevance of emodin in lung cancer models. Tang et al. reported that carrier-free self-assembled doxorubicin/emodin nanoparticles showed synergistic cytotoxicity in A549 non-small-cell lung cancer cells, improved *in vivo* antitumor efficacy, and suppressed efflux-pump-associated drug resistance through inhibition of p65 activation and nuclear translocation [28]. Although that study used a nanoparticle combination strategy, it supports the broader interpretation that emodin can contribute to lung cancer growth inhibition and modulation of therapy-resistance-associated signaling. The suppression of insulin-associated PI3K/Akt/mTOR signaling observed in the present study is also consistent with previous breast cancer work. Ponnusamy et al. reported that emodin, particularly in combination with berberine, inhibited SIK3-associated mTOR/Akt signaling, reduced breast cancer cell growth, and promoted apoptosis [11]. In parallel, Zheng et al. summarized evidence that emodin can inhibit HIF-1 biosynthesis and exert anticancer effects through suppression of PI3K/AKT and ERK signaling [26]. These reports support the relevance of our $CoCl_2$ and insulin-stimulation experiments, where emodin reduced HIF-1α accumulation and modulated PI3K/Akt/mTOR-associated responses. Emodin influenced mTOR-associated signaling, although the magnitude and direction of the effect may depend on cell type, stimulation context, and treatment timing. Such context dependence is not unexpected for PI3K/Akt/mTOR biology, where feedback loops and compensatory signaling can alter downstream readouts.

The migration data provide a separate view of tumor aggressiveness. MDA-MB-231 cells are an appropriate model for this endpoint because they represent a triple-negative breast cancer phenotype with high motility and invasive potential. Dactolisib caused the strongest suppression of migration-associated cell index, as expected for a direct PI3K/mTOR-targeted inhibitor. ROE and emodin produced more moderate attenuation under the tested conditions. This pattern is biologically plausible: in the present design, the most pronounced effects of ROE and emodin were observed on viability and proliferative fitness, while migration was less strongly affected. Published evidence showing emodin inhibition of MDA-MB-231 migration and invasion supports the relevance of this endpoint and justifies additional optimization of dose, timing, and invasion-specific conditions in future studies [13, 29]. The moderate antimigratory effect observed in our xCELLigence migration assay should be interpreted together with previous MDA-MB-231 data. Sun et al. demonstrated that emodin dose-dependently inhibited migration, invasion, and lung metastasis of MDA-MB-231 breast cancer cells, with reduced MMP-2, MMP-9, uPA, and uPAR expression and decreased p38/ERK activity [13]. This is relevant to the obtained data because MMP-2 was included among the docking targets and showed a favorable predicted interaction with emodin. More recent breast cancer data also support an anti-migratory and tumor microenvironment-modulating role for emodin: Liu et al. reported that emodin inhibited breast cancer cell stemness, migration, macrophage infiltration, angiogenesis, IL-17 expression, and tumor growth under hyperlipidemic conditions [16]. Therefore, although migration inhibition was less

pronounced than cytotoxicity and signaling modulation under our experimental conditions, the MDA-MB-231 migration endpoint remains mechanistically justified and literature-supported.

The current findings also align with the emerging concept that plant-derived polyphenol-rich preparations and pathway modulators may influence not only tumor cells directly, but also the pro-metastatic microenvironment. In our recent study focused on the bone-marrow niche, polyphenol-enriched plant extracts and pathway modulators attenuated HIF-1α, COX-2 and MMP-2 expression in cancer-cell models and reduced TNF-α-driven migration/invasion, supporting the relevance of the hypoxia–inflammation–matrix remodeling axis in breast-cancer progression [23]. This concept is important for the present study, taking into account that emodin reduced HIF-1α and influenced PI3K/mTOR-associated signaling, while ROE has already been shown in earlier work to affect inflammatory and matrix-remodeling mediators. Thus, the present data position emodin within a broader ROE-associated anticancer network involving survival signaling, apoptosis, hypoxia adaptation, and tumor-promoting microenvironmental cues.

The translational implications of our findings are twofold. First, ROE remains a valuable anticancer phytochemical preparation whose biological activity can be further standardized through chemical profiling, bioactivity-guided fractionation, and mechanistic validation. Second, emodin can be advanced as a defined candidate compound. Its advantages are a known chemical structure, reported anticancer activity across several tumor types, and mechanistic alignment with PI3K/Akt/HIF-1α/apoptosis-associated signaling. At the same time, further development of emodin will require attention to known pharmacological limitations, including bioavailability and safety considerations described in recent reviews [10, 14]. These limitations do not reduce the value of emodin as a lead candidate; rather, they define the next translational tasks, including formulation development, dose optimization, selectivity testing, and *in vivo* efficacy validation.

5. Conclusion

This study confirms the anticancer efficiency of *R. obtusifolius* seed ethanol extract and advances emodin as a defined ROE-associated compound with relevant cytotoxic, apoptosis-associated, and pathway-modulating activity. ROE reduced MCF-7 breast cancer cell viability, impaired real-time proliferative fitness, and increased membrane-compromised cells, confirming its reproducible anticancer activity in a breast cancer model. Emodin reproduced important components of this phenotype by suppressing real-time proliferative fitness, increasing membrane-compromised cells, enhancing caspase-3-associated apoptotic signaling, attenuating insulin-induced PI3K/Akt activation, influencing mTOR-associated responses, and suppressing $CoCl_2$-induced HIF-1α accumulation. The migration data further suggest a moderate attenuation of aggressive cell behavior, although this effect was weaker than the cytotoxic and signaling responses under the applied conditions. Overall, the findings support a model in which ROE acts as a multi-component anticancer phytochemical matrix, while emodin represents a rational compound-level candidate contributing to survival-pathway inhibition, hypoxia-response modulation, and apoptosis-associated effects. As the present dataset is based on in vitro and in silico

approaches, future work should include ROE–emodin comparative pathway validation, normal-cell selectivity testing, and in vivo efficacy and tolerability studies.

Abbreviations

Akt, protein kinase B; ANOVA, analysis of variance; ATCC, American Type Culture Collection; AUC, area under the curve; Bcl-2, B-cell lymphoma 2; BEZ235, dactolisib; CI, cell index; $CoCl_2$, cobalt chloride; COX-2, cyclooxygenase-2; DAPI, 4',6-diamidino-2-phenylindole; DMBA, 7,12-dimethylbenz[a]anthracene; DMEM, Dulbecco's modified Eagle's medium; DMSO, dimethyl sulfoxide; DOX, doxorubicin; DW, dry weight; FBS, fetal bovine serum; HIF-1α, hypoxia-inducible factor 1-alpha; HPLC, high-performance liquid chromatography; ICC, immunocytochemistry; IC_{50}, half-maximal inhibitory concentration; KEGG, Kyoto Encyclopedia of Genes and Genomes; LC-HRMS, liquid chromatography–high-resolution mass spectrometry; MAPK, mitogen-activated protein kinase; MMP-2, matrix metalloproteinase-2; mTOR, mechanistic target of rapamycin; MTT, 3-(4,5-dimethylthiazol-2-yl)-2,5-diphenyltetrazolium bromide; NF-κB, nuclear factor kappa B; PBS, phosphate-buffered saline; PDB, Protein Data Bank; PI3K, phosphoinositide 3-kinase; PPI, protein–protein interaction; pAKT, phosphorylated AKT; pPI3K, phosphorylated PI3K; RO, *Rumex obtusifolius*; ROE, *Rumex obtusifolius* seed ethanol extract; ROS/RNS, reactive oxygen/nitrogen species; RTCA, real-time cell analysis; SD, standard deviation; SEM, standard error of the mean; TNF-α, tumor necrosis factor alpha; VEGF-α, vascular endothelial growth factor alpha.

Declarations

Data availability

The data supporting the findings of this study are available from the corresponding author upon reasonable request. Previously published phytochemical and biological datasets are cited in the manuscript.

Ethics statement

The current manuscript is based on *in vitro* cancer-cell experiments and *in silico* analyses. No human participants or live vertebrate animals were used in the experimental dataset described here.

Author Contributions

HG, MG, NA, and AM conceptualized and supervised the study, prepared the original draft, and performed manuscript reviewing and editing. MK conducted the *in silico* analyses. EN and NA performed the ICC experiments. GP and SH carried out the RTCA experiments. All authors read and approved the final version of the manuscript.

Funding

This work was supported by the Higher Education and Science Committee of MESCS RA Research projects numbered 23LCG-1F010 and 24WS-1F036.

Conflict of interest

The authors declare no competing interests.

References

1. Newman, D. J. & Cragg, G. M. Natural Products as Sources of New Drugs over the Nearly Four Decades from 01/1981 to 09/2019. *J. Nat. Prod.* **83**, 770–803 (2020).
2. Hanahan, D. Hallmarks of Cancer: New Dimensions. *Cancer Discov*. **12**, 31–46 (2022).
3. Peng, Y., Wang, Y., Zhou, C., Mei, W. & Zeng, C. PI3K/Akt/mTOR Pathway and Its Role in Cancer Therapeutics: Are We Making Headway? *Front Oncol* **12**, (2022).
4. Basheeruddin, M., Qausain, S. & Hypoxia-Inducible Factor 1-Alpha (HIF-1α) and Cancer: Mechanisms of Tumor Hypoxia and Therapeutic Targeting. *Cureus* (2024). https://doi.org/10.7759/cureus.70700 doi:10.7759/cureus.70700.
5. Yong, L. et al. The role of hypoxia-inducible factor-1 alpha in multidrug-resistant breast cancer. *Front Oncol* **12**, (2022).
6. Ginovyan, M., Sahakyan, N., Aghajanyan, A. & Trchounian, A. Antioxidant potential, biochemical activity and hypoglycemic effects of R. obtusifolius L. seed extracts used in Armenian traditional medicine. *BIO Web Conf.* **30**, 05001 (2021).
7. Ginovyan, M., Ayvazyan, A., Nikoyan, A., Tumanyan, L. & Trchounian, A. Phytochemical Screening and Detection of Antibacterial Components from Crude Extracts of Some Armenian Herbs Using TLC-Bioautographic Technique. *Curr. Microbiol.* **77**, 1223–1232 (2020).
8. Ginovyan, M. et al. Anti-cancer effect of Rumex obtusifolius in combination with arginase/nitric oxide synthase inhibitors via downregulation of oxidative stress, inflammation, and polyamine synthesis. *International J. Biochem. Cell. Biology* **158**, (2023).
9. Ginovyan, M. et al. 5-fluorouracil and Rumex obtusifolius extract combination trigger A549 cancer cell apoptosis: uncovering PI3K/Akt inhibition by in vitro and in silico approaches. *Sci. Rep.* **14**, 14676 (2024).
10. Akkol, E. K. et al. Is Emodin with Anticancer Effects Completely Innocent? Two Sides of the Coin. *Cancers (Basel)*. **13**, 2733 (2021).
11. Ponnusamy, L., Kothandan, G. & Manoharan, R. Berberine and Emodin abrogates breast cancer growth and facilitates apoptosis through inactivation of SIK3-induced mTOR and Akt signaling pathway. *Biochim. et Biophys. Acta (BBA) - Mol. Basis Disease*. **1866**, 165897 (2020).
12. Sui, J. Q., Xie, K. P., Zou, W. & Xie, M. J. Emodin Inhibits Breast Cancer Cell Proliferation through the ERα-MAPK/Akt-Cyclin D1/Bcl-2 Signaling Pathway. *Asian Pac. J. Cancer Prev.* **15**, 6247–6251 (2014).

13. Sun, Y. et al. Inhibitory effect of emodin on migration, invasion and metastasis of human breast cancer MDA-MB-231 cells in vitro and in vivo. *Oncol. Rep.* **33**, 338–346 (2015).
14. Zhang, Q. et al. The versatile emodin: A natural easily acquired anthraquinone possesses promising anticancer properties against a variety of cancers. *Int. J. Biol. Sci.* **18**, 3498–3527 (2022).
15. Yuan, G., Mao, J. & Li, Z. Systematically investigate the mechanism underlying the therapeutic effect of emodin in treatment of prostate cancer. *Discover Oncol.* **16**, 413 (2025).
16. Liu, Q. et al. Emodin inhibits breast tumorigenesis in the comorbidity of hyperlipidemia and associated with IL-17 suppression. *Biochem. Biophys. Rep.* **45**, 102520 (2026).
17. Ginovyan, M., Petrosyan, M. & Trchounian, A. Antimicrobial activity of some plant materials used in Armenian traditional medicine. *BMC Complement. Altern. Med.* **17**, 1–9 (2017).
18. Javrushyan, H. et al. Elucidating the impact of Hypericum alpestre extract and L-NAME on the PI3K/Akt signaling pathway in A549 lung adenocarcinoma and MDA-MB-231 triple-negative breast cancer cells. *PLoS One*. **20**, e0303736 (2025).
19. Yang, J. et al. Inhibition of PI3K-AKT signaling blocks PGE2-induced COX-2 expression in lung adenocarcinoma. *Onco Targets Ther.* **13**, 8197–8208 (2020).
20. Pang, L. et al. Cox-2 Inhibition Protects against Hypoxia/Reoxygenation-Induced Cardiomyocyte Apoptosis via Akt-Dependent Enhancement of iNOS Expression. *Oxid. Med. Cell. Longev.* (2016). (2016).
21. Trott, O., Olson, A. J., AutoDock & Vina Improving the speed and accuracy of docking with a new scoring function, efficient optimization, and multithreading. *J. Comput. Chem.* **31**, 455–461 (2010).
22. Ginovyan, M. et al. Hypericum alpestre extract exhibits in vitro and in vivo anticancer properties by regulating the cellular antioxidant system and metabolic pathway of L-arginine. *Cell Biochem. Funct* **42**, (2024).
23. Javrushyan, H. et al. Evaluating the Efficacy of Polyphenol-Enriched Plant Extracts and Pathway Modulators in the Bone Marrow to Suppress Breast Cancer Progression. *The FASEB Journal* **40**, (2026).
24. Javrushyan, H. et al. Evaluating the Efficacy of Polyphenol-Enriched Plant Extracts and Pathway Modulators in the Bone Marrow to Suppress Breast Cancer Progression. *The FASEB Journal* **40**, (2026).
25. Zhang, S. et al. Comparative Study of Three Raspberry Cultivar (Rubus idaeus L.) LeavesMetabolites: Metabolome Profiling andAntioxidantActivities. *Applied Sci. (Switzerland)* **12**, (2022).
26. Zheng, Q., Li, S., Li, X. & Liu, R. Advances in the study of emodin: an update on pharmacological properties and mechanistic basis. *Chin. Med.* **16**, 102 (2021).
27. Su, Y. T., Chang, H. L., Shyue, S. K. & Hsu, S. L. Emodin induces apoptosis in human lung adenocarcinoma cells through a reactive oxygen species-dependent mitochondrial signaling pathway. *Biochem. Pharmacol.* **70**, 229–241 (2005).

28. Tang, C. et al. Synergistic anticancer effects of carrier-free self-assembled doxorubicin and emodin nanoparticles in non-small cell lung cancer. *Sci. Rep.* **15**, 40205 (2025).
29. Li, F., Song, X., Zhou, X., Chen, L. & Zheng, J. Emodin attenuates high lipid-induced liver metastasis through the AKT and ERK pathways in vitro in breast cancer cells and in a mouse xenograft model. *Heliyon* **9**, e17052 (2023).

Figures

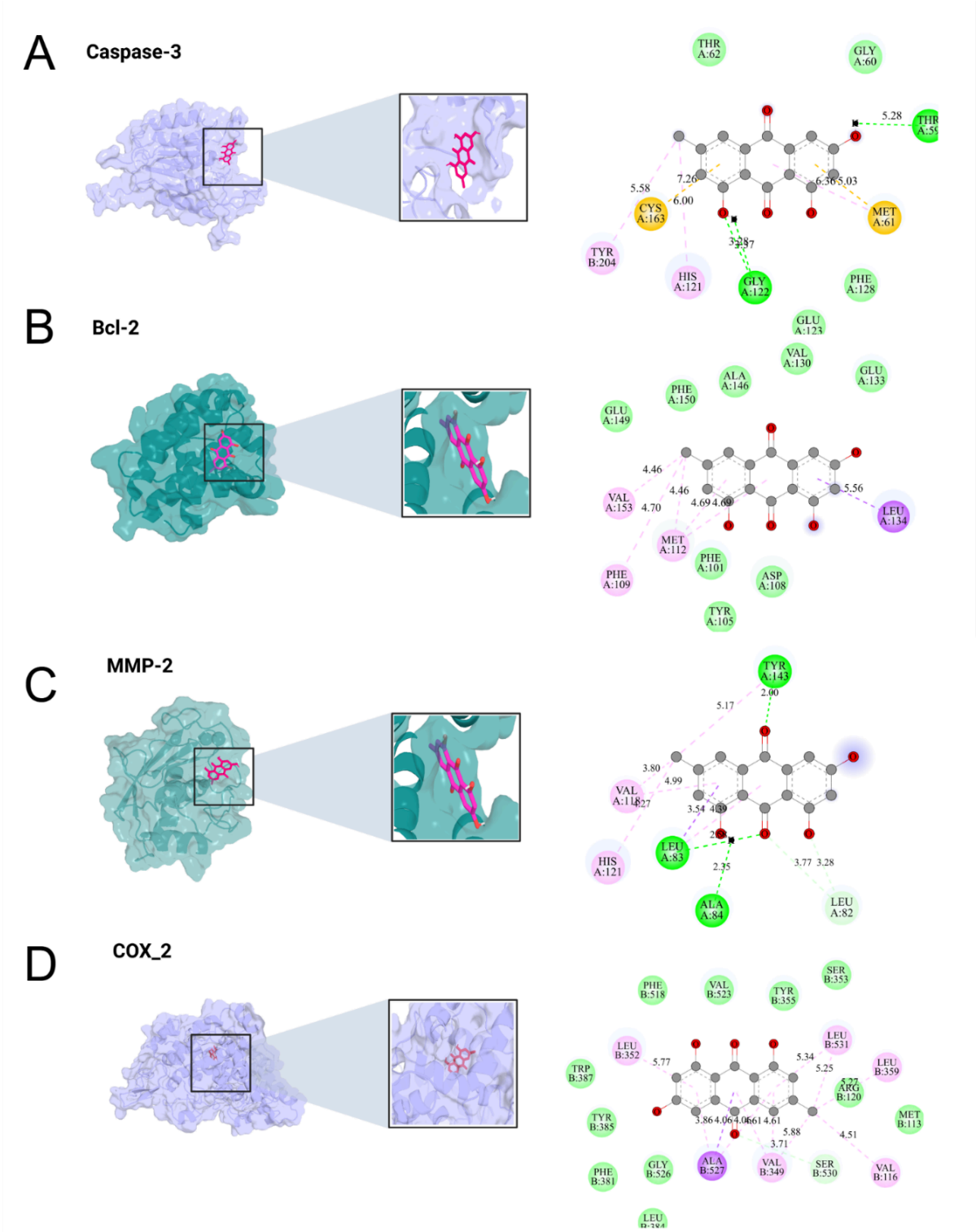

Figure 1

Molecular docking analysis of emodin with apoptosis-, inflammation-, and invasion-associated target proteins. Predicted three-dimensional binding poses and corresponding two-dimensional interaction diagrams of emodin with caspase-3 (A), Bcl-2 (B), MMP-2 (C), and COX-2 (D) are shown. The docking analysis indicates that emodin can be accommodated within functionally relevant binding regions of these proteins. In the two-dimensional diagrams, green dashed lines indicate conventional hydrogen

bonds, light-green dashed lines indicate carbon–hydrogen bonds, purple dashed lines indicate π–sigma interactions, and pink dashed lines indicate hydrophobic interactions, including alkyl and π–alkyl contacts.

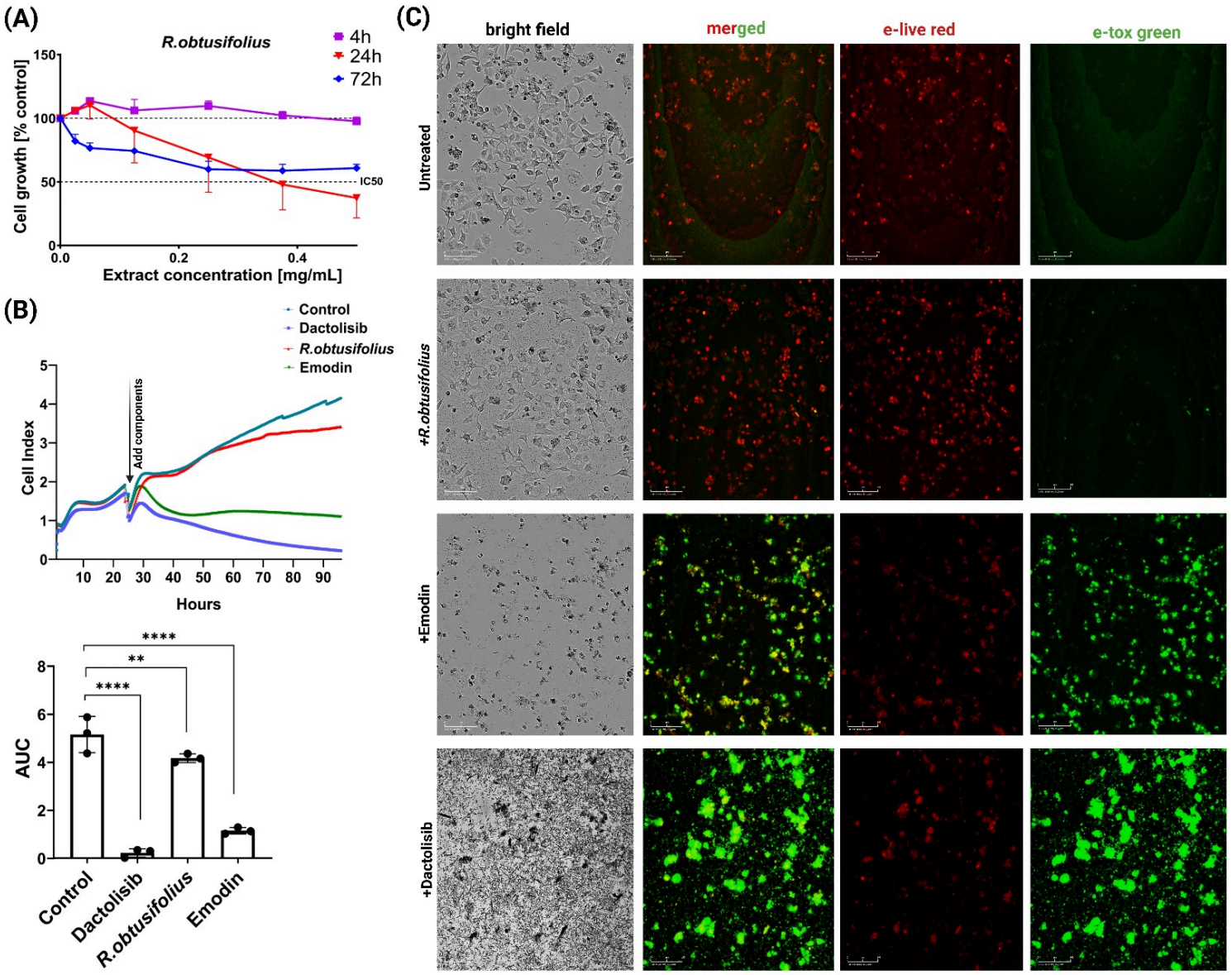

Figure 2

ROE and emodin impair MCF-7 breast cancer cell viability and real-time proliferative fitness. (A) MTT dose–response analysis of ROE in MCF-7 cells after 4, 24, and 72 h of exposure. The dashed line indicates 50% cell growth/viability relative to the untreated control and was used to estimate the IC_{50} threshold. ROE produced a time- and concentration-dependent reduction in cell growth, with the strongest effect observed after prolonged exposure. (B) Representative xCELLigence RTCA impedance-based proliferation curves showing dynamic changes in Cell Index after treatment with ROE, emodin, or the PI3K/mTOR inhibitor dactolisib. Treatments were added 24 h after seeding, as indicated by the arrow. AUC quantification demonstrates treatment-associated reduction in proliferative capacity, with dactolisib and emodin showing the most pronounced suppression. (C)

Representative live-cell imaging after 72 h of treatment. Bright-field, merged fluorescence, e-Live Red, and e-Tox Green channels are shown. Increased e-Tox Green fluorescence indicates plasma membrane compromise and loss of cell viability, particularly after emodin and dactolisib treatment. At the same time, ROE induced a moderate cytotoxic signal compared with untreated cells. Data are presented as mean ± SD. Statistical significance was determined by one-way ANOVA followed by Tukey's multiple-comparison test. **p < 0.01, ****p < 0.0001. Scale bars are shown on the images.

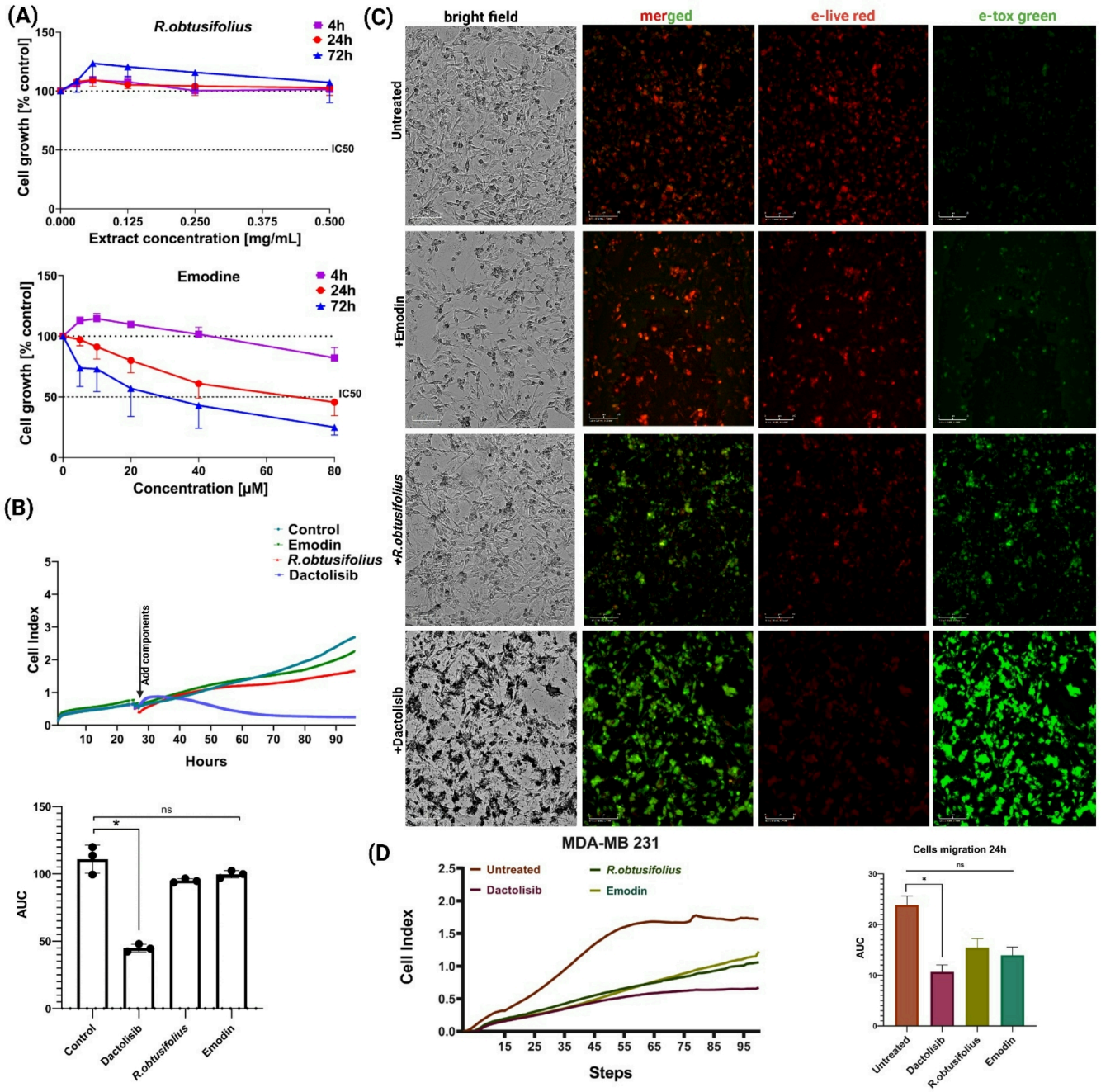

Figure 3

ROE and emodin differentially affect MDA-MB-231 breast cancer cell viability, proliferative fitness, and migration. (A) MTT dose–response analysis of ROE and emodin in MDA-MB-231 cells after 4, 24, and 72 h of treatment. ROE showed limited direct anti-viability activity within the tested concentration range, whereas emodin produced a time- and concentration-dependent reduction in cell growth, with the strongest effect after 72 h. (B) Real-time xCELLigence RTCA impedance-based proliferation profiles and AUC quantification showing treatment-associated changes in Cell Index after exposure to ROE, emodin, or dactolisib. Dactolisib produced the strongest suppression, while ROE and emodin showed more moderate effects on proliferation-associated impedance. (C) Representative bright-field and live-cell fluorescence images after 72 h of treatment. e-Live Red marks viable cells, whereas e-Tox Green indicates membrane-compromised/dead cells. Dactolisib induced the strongest cytotoxic signal, while ROE and emodin increased membrane-compromised cells compared with the untreated control. (D) Real-time xCELLigence CIM-plate migration analysis and 24-h AUC quantification. Dactolisib markedly reduced migration-associated Cell Index, whereas ROE and emodin produced moderate, non-significant attenuation of migration under the applied conditions. Data are presented as mean ± SD. Statistical significance was assessed by one-way ANOVA followed by Tukey's multiple-comparison test. *p < 0.05; ns, not significant. Scale bars are shown on the images.

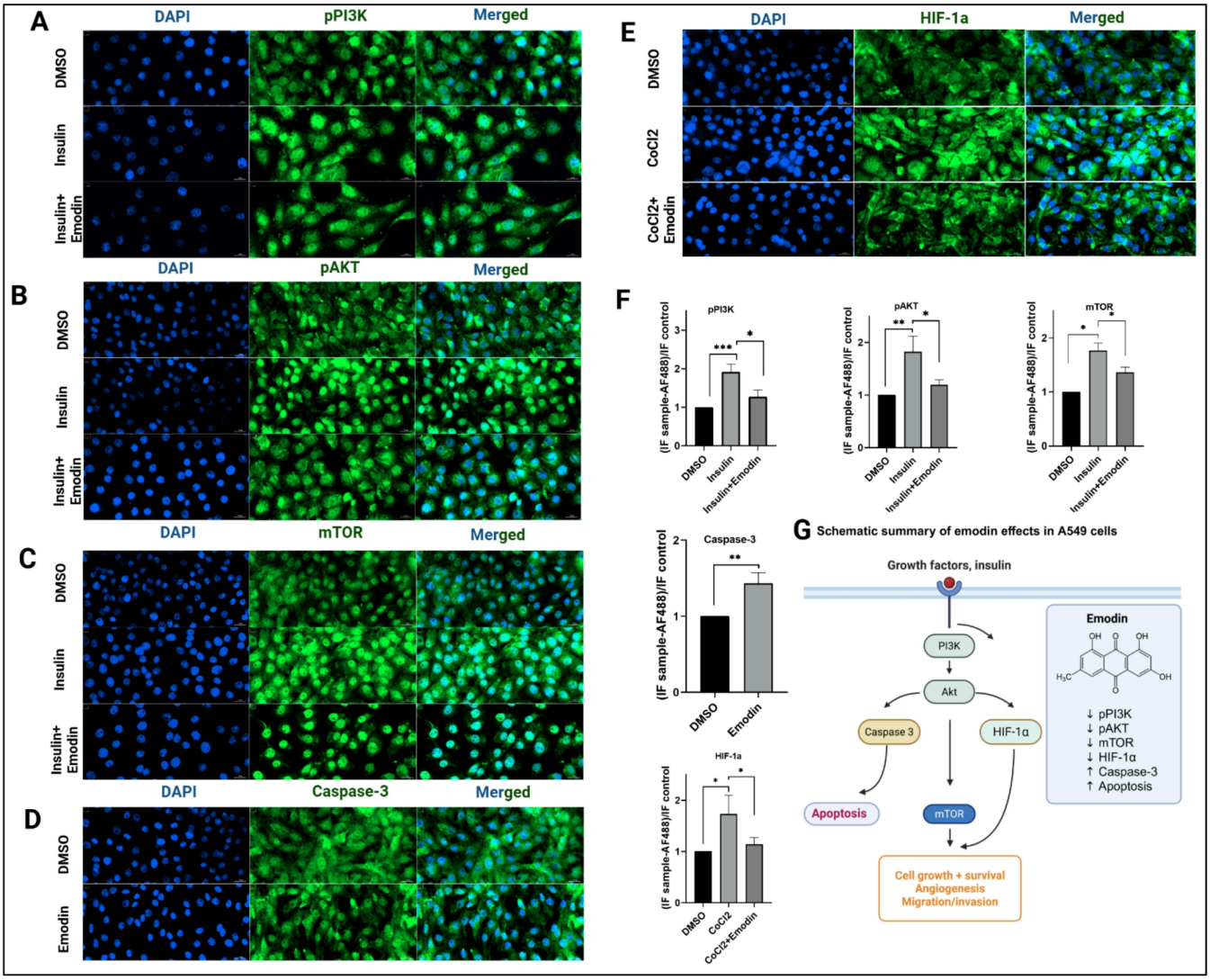

Figure 4

Emodin suppresses insulin-driven PI3K/Akt/mTOR signaling and modulates apoptosis- and hypoxia-associated responses in A549 lung adenocarcinoma cells. (A–E) Representative immunofluorescence micrographs of A549 cells treated with vehicle control (DMSO), insulin, emodin, $CoCl_2$, and doxorubicin (DOX), as indicated. Nuclei were counterstained with DAPI/Hoechst (blue), and target proteins were detected using Alexa Fluor-conjugated secondary antibodies (green). Merged images are shown in the corresponding panels. (A) Phosphorylated PI3K (pPI3K). (B) Phosphorylated AKT (pAKT). (C) mTOR. (D) Cleaved caspase-3. (E) HIF-1α. (F) Quantitative fluorescence intensity analysis normalized to vehicle-treated control cells (DMSO = 1), (G) Schematic summary of emodin effects in A549 cells. Emodin attenuated insulin-induced PI3K/Akt/mTOR signaling and reduced $CoCl_2$-induced HIF-1α accumulation, while increasing caspase-3-associated apoptotic signaling, indicating suppression of survival- and hypoxia-associated pathways together with promotion of apoptosis. Insulin was used to stimulate PI3K/Akt/mTOR signaling, $CoCl_2$ served as a positive control for hypoxia-mimetic induction

of HIF-1α, and doxorubicin was included as a positive control for apoptosis in caspase-3 experiments. Emodin reduced insulin-induced pPI3K and pAKT signals, showed a moderate inhibitory effect on insulin-associated mTOR activation, increased caspase-3 immunofluorescence, and attenuated $CoCl_2$-induced HIF-1α accumulation. Data are presented as mean ± SEM from three independent biological experiments. In each experiment, cells were plated in three separate wells per condition, and eight random microscopic fields were analyzed per well. Quantified values represent pooled means of all replicates. Statistical significance was determined by one-way ANOVA followed by appropriate post hoc multiple-comparison testing. *p < 0.05, **p < 0.01, ***p < 0.001, ****p < 0.0001; ns, not significant. Magnification: 20×; scale bar: 20 μm.

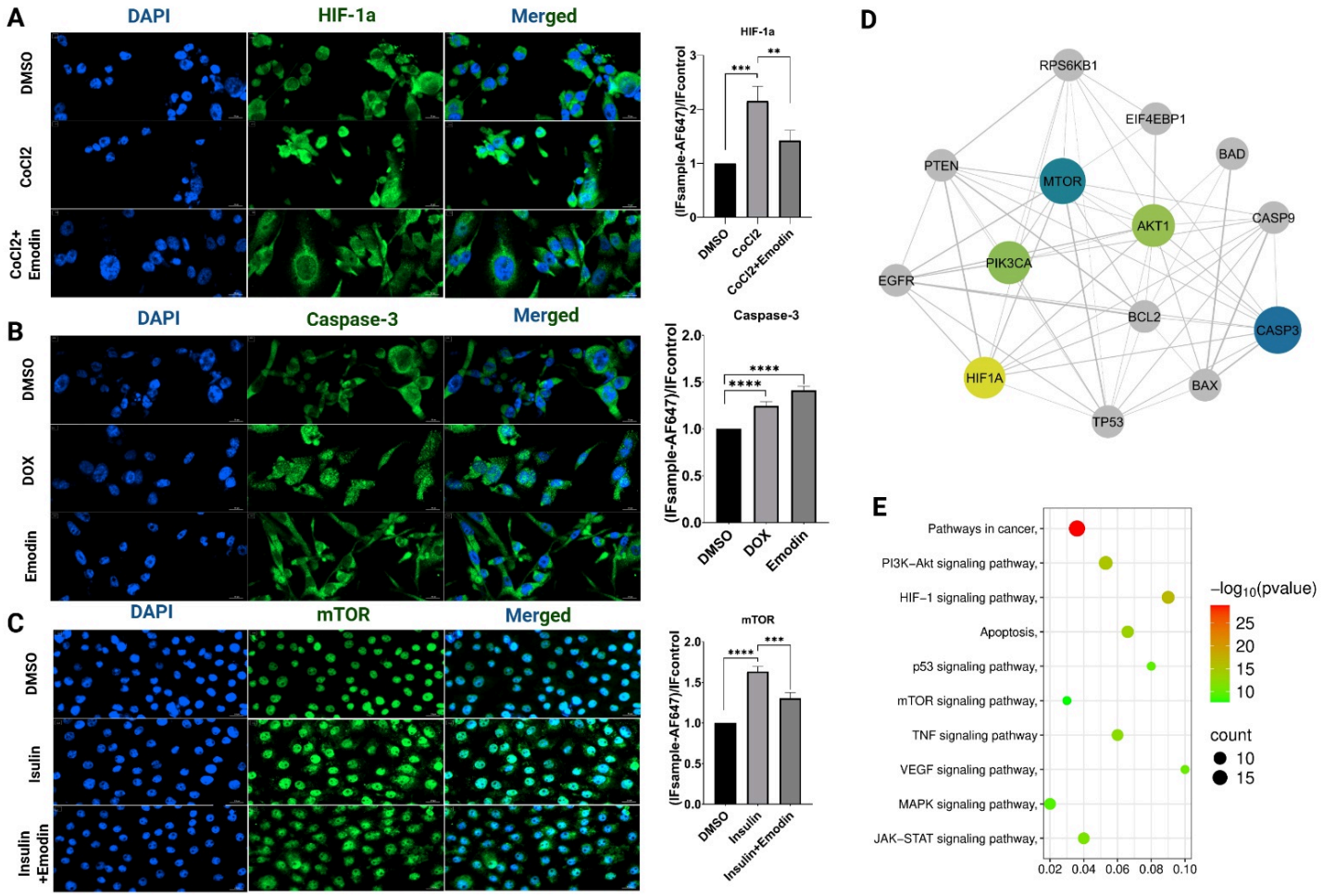

Figure 5

Emodin modulates hypoxia-, apoptosis-, and mTOR-associated responses in MDA-MB-231 triple-negative breast cancer cells and is linked to cancer-relevant signaling networks. (A–C) Representative immunofluorescence micrographs and quantitative fluorescence analysis of MDA-MB-231 cells treated with vehicle control (1% DMSO), insulin, emodin, $CoCl_2$, or doxorubicin (DOX), as indicated. Nuclei were counterstained with DAPI/Hoechst (blue), and target proteins were detected using Alexa Fluor-conjugated secondary antibodies (green). Merged images are shown in the corresponding

panels. (A) HIF-1α expression under $CoCl_2$-induced hypoxia-mimetic stress. $CoCl_2$ increased HIF-1α signal, whereas co-treatment with emodin attenuated the $CoCl_2$-induced HIF-1α response. (B) Caspase-3 expression after treatment with emodin or doxorubicin. Doxorubicin was used as a pro-apoptotic positive control, while emodin increased caspase-3-associated immunofluorescence compared with vehicle-treated control cells. (C) mTOR expression under insulin-stimulated growth/survival signaling. Insulin increased mTOR immunofluorescence, whereas co-treatment with emodin reduced the insulin-associated mTOR signal. (D) Protein–protein interaction (PPI) network of emodin-associated targets constructed and visualized using Cytoscape. The network illustrates functional connectivity among predicted or selected emodin-related targets and highlights key cancer-associated signaling nodes potentially involved in the observed cellular effects. (E) KEGG pathway enrichment analysis of emodin-associated target genes/proteins, showing major biological pathways potentially involved in its anticancer activity, including cancer-related signaling, survival, apoptosis, inflammatory/hypoxia-associated, and PI3K/Akt/mTOR-linked pathways. Data are presented as mean ± SEM from three independent biological experiments. In each experiment, cells were plated in three separate wells per condition, and eight random microscopic fields were analyzed per well. Statistical significance was determined by one-way ANOVA followed by appropriate post hoc multiple-comparison testing. *p < 0.05, **p < 0.01, ***p < 0.001, ****p < 0.0001; ns, not significant. Magnification: 20×; scale bar: 20 μm (mTOR: 100 μm).

Supplementary Files

This is a list of supplementary files associated with this preprint. Click to download.

- Suppl.tab1.docx